Med Biol Eng Comput (2014) 52:353–362
DOI 10.1007/s11517-014-1142-1

ORIGINAL ARTICLE

Object-shape recognition and 3D reconstruction from tactile sensor images

Anwesha Khasnobish · Garima Singh · Arindam Jati · Amit Konar · D. N. Tibarewala

Received: 2 April 2013 / Accepted: 17 January 2014 / Published online: 28 January 2014

Abstract This article presents a novel approach of edged and edgeless object-shape recognition and 3D reconstruction from gradient-based analysis of tactile images. We recognize an object's shape by visualizing a surface topology in our mind while grasping the object in our palm and also taking help from our past experience of exploring similar kind of objects. The proposed hybrid recognition strategy works in similar way in two stages. In the first stage, conventional object-shape recognition using linear support vector machine classifier is performed where regional descriptors features have been extracted from the tactile image. A 3D shape reconstruction is also performed depending upon the edged or edgeless objects classified from the tactile images. In the second stage, the hybrid recognition scheme utilizes the feature set comprising both the previously obtained regional descriptors features and some gradient-related information from the reconstructed object-shape image for the final recognition in corresponding four classes of objects viz. planar, one-edged object, two-edged object and cylindrical objects. The hybrid strategy achieves 97.62 % classification accuracy, while the conventional recognition scheme reaches only to 92.60 %. Moreover, the proposed algorithm has been proved to be less noise prone and more statistically robust.

Keywords Pattern recognition · Object-shape recognition · Haptic recognition · Image processing · Tactile image

A. Khasnobish (✉) · D. N. Tibarewala
School of Bioscience and Engineering, Jadavpur University, Kolkata, India
e-mail: anweshakhasno@gmail.com

G. Singh · A. Jati · A. Konar
Department of Electronics and Telecommunication Engineering, Jadavpur University, Kolkata, India

1 Introduction

Haptic perception is the phenomenon of understanding real-world objects by physical contact of our palm or any other body parts. We can perceive the shape, size, texture, hardness and many other properties of an object just by touching or gripping it with our palm. This process helps us recognizing objects around us. Unfortunately, the disabled people using conventional upper-limb prosthetics are unable to capture shape information of objects by acquiring sensory touch signals. Prosthetic devices currently employed as artificial limb cannot perceive shape information by proximity analysis. Thus, designing artificial tactile sensory systems and incorporating them into robotic hands will not only help the disabled but also can be used in various human–computer interactions.

We have formulated an approach of artificial touch sensation for robotic arms consisting of two parts. The first part will consist of an artificial palm attached with tactile sensors that are capable of acquiring the pressure distribution pattern of an object when it is gripped in that palm. Then, the object's shape is recognized and reconstructed from analyzing the raw pressure distribution. In the second part, the recognized object shape is transferred to the subject (the amputee) through a vibrotactile actuator to any of his/her active muscle. The vibrotactile feedback will help people with somatosensory failure or with lost upper limb to have a sensation of the grasp or explorations force, which will in turn lead to enhanced controllability to maneuver the artificial arms. The prerequisite of developing such system is the recognition of the objects' shape from the raw pressure distribution pattern (generally known as *haptic recognition*) and the 3D reconstruction of that shape. The present work is dedicated for this part.

The literature shows a decent number of papers in the field of developing devices capable of having haptic sensation [11, 28]. Sigiuchi et. al. [23] developed the control system for a multi-fingered robotic hand with distributed touch sensor. Similar touch sensitive robotic arms were developed in the recent past [2, 5, 18, 21, 22, 26, 27]. Simpkins et al. [24] presented a survey of the state-of-art of robotic tactile sensing. Object-shape classification technique based on tactile information using universal robotic hand was proposed in [18]. Similar haptic recognition schemes using multiple samples/grasping were proposed in [12,14, 19, 20, 25]. Object-shape reconstructions are performed from tactile images [3, 15] and also from images of the objects itself [4]. Yamada et. al. [30] proposed a method of 3D object reconstruction from both visual and tactile data using internal models with global and local deformations.

But, the literature lacks a fast and accurate method of object-shape recognition and 3D reconstruction which can be embedded into a microcontroller and which, along with the vibrotactile actuator, can help us implementing the artificial haptic perception system discussed previously. The reasons behind this are (1) time delay due to multiple grasping for recognition, (2) the absence of the 3D reconstruction process which is needed for the vibrotactile actuator to reproduce the 3D shape of the object that is in grip of the robotic/prosthetic palm, (3) lack of suitable algorithms having high recognition accuracy which is needed to deal with a large number of objects having similar complex shapes, and (4) the use of multisensory data fusion in recognition and reconstruction. Therefore, keeping in mind the necessity for the proposed application-oriented problem, we are going to present a simple, fast and useful haptic recognition scheme along with a 3D shape reconstruction technique.

The article presents a novel technique of edged and edgeless object-shape recognition as well as 3D reconstruction of the portion of the object under grasp from tactile images obtained by commercially available tactile sensor array. At the initial stage of the research, the objects have been grasped by normal human palm attached with the sensor array due to the lack of proper robotic palm. Besides the proposition of recognition and reconstruction algorithms, the article presents a hybrid approach of object-shape recognition from tactile images by combining the initial recognition and reconstruction stages. When we try to recognize an object just by holding it in our palm, we not only use our perception about the pressure distribution produced on the palm (and therefore making a visual 3D image of the object in the mind) but also try to recognize it based on our past experience, i.e., learning from previous encounters with the same object. These two phenomena when combined together provide a better recognition of the object's shape. Here, we try to mimic this natural phenomenon to develop a hybrid shape recognition algorithm for achieving higher recognition accuracy. Generally, in object-shape recognition problems, some features are extracted from the image, which are utilized for classification, i.e., conventional recognition. Here, the recognition is carried out in two stages: (1) Some regional features are extracted from the tactile image, and (2) Some shape-related features are extracted from the 3D-reconstructed object-shape image. These two feature vectors are combined to construct a high-dimensional feature vector that is then applied to the classifier for recognition.

The experiment is performed using four generic object-shape classes viz. (1) planar, (2) object having one edge, (3) object having two edges (i.e., when a cuboid is gripped) and (4) cylindrical object. Our choice of objects encompasses the generic shapes (or surfaces) we commonly encounter in our surroundings or the shapes whose combination gives rise to a more complex-shaped object. In the first stage of the algorithm, some *regional descriptors* [8, 13] extracted from the tactile image have been used as features for recognition. The reconstruction algorithm uses a pretrained classifier to determine whether an object is edged or edgeless and therefore reconstruct its 3D shape applying two different strategies. In the second stage, the regional descriptors and some gradient-related features extracted from the reconstructed object-shape images are combined with the previously extracted regional descriptor features, to form a high-dimensional feature vector, which is then classified in corresponding object-shape classes. The two-stage hybrid shape recognition algorithm mimics human strategy of shape recognition and is shown in the form of a flowchart in Fig. 1. The novelties of the proposed method are given below.

1. The proposed scheme describes a simple and fast haptic recognition technique that can be suitably embedded in a haptic perception system consisting of a haptic recognition system and a vibrotactile actuator.
2. Rather than considering multiple tactile images, our technique is capable of recognizing the object and reconstructing the 3D shape of the portion of the object in grip from a single tactile image. Therefore, the proposed scheme is fast and suitable for real-time implementation.
3. The hybrid recognition algorithm mimics the natural object recognition technique of humans and provides very high recognition accuracy.

The rest of the article is organized as follows. The Sect. 2 presents the shape recognition technique where only

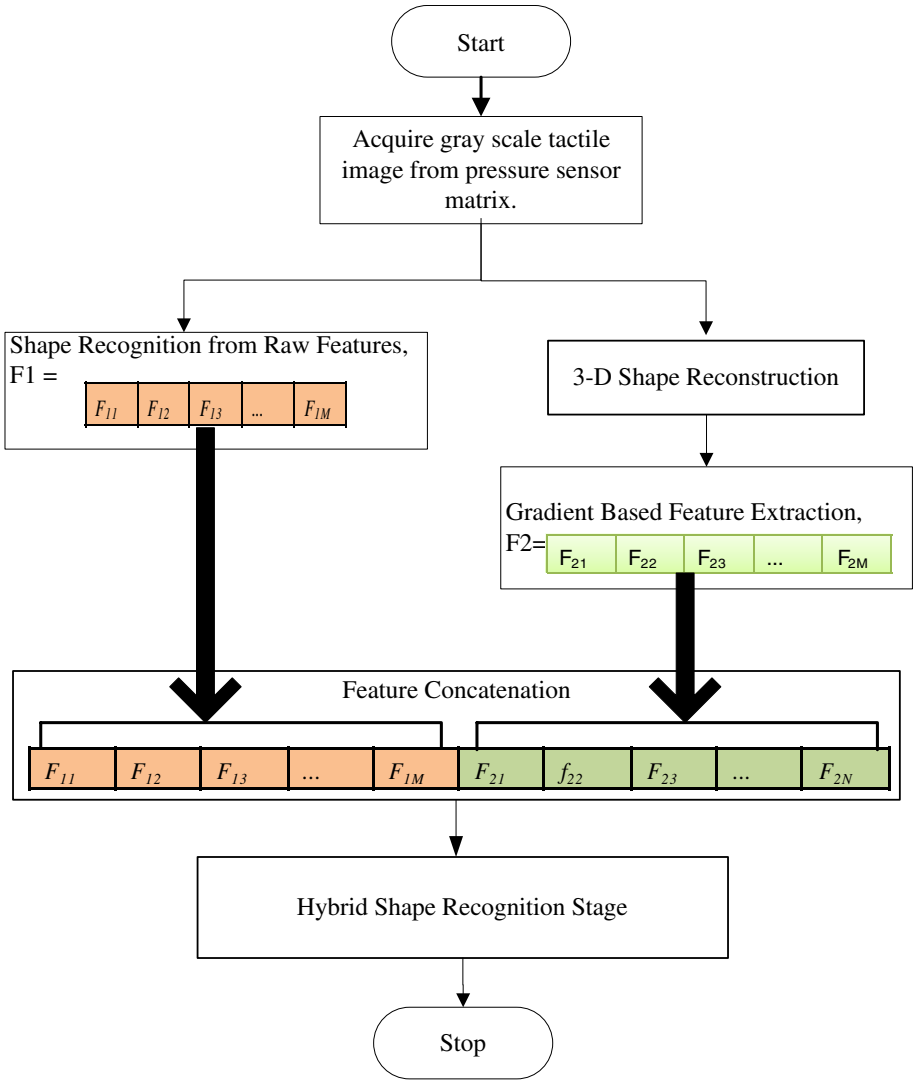

Fig. 1 The hybrid object-shape recognition algorithm

regional descriptors are used as features, followed by the 3D shape reconstruction algorithm in Sect. 3 and the hybrid shape recognition algorithm in Sect. 4. Results and conclusions are presented in the concluding Sects. 5 and 6, respectively.

2 Object-shape recognition from tactile image features

2.1 Experimental paradigm

The tactile image acquisition method makes use of commercially available tactile sensor array. We have used a 32 × 32 tactile array of sensors developed by pressure profile systems (PPS) (software version—Chameleon software). Fifty subjects of age group 23 ± 3 years took part in the experiment after signing up a consent form. The subjects grasped the objects with his/her natural grasping force holding the objects with their palm pointing downwards (as shown in Fig. 2a). A total of 4,000 images (50 subjects grasped four classes of objects ten times with each of left and right palm, thus 80 images per subject) have been acquired for each of the aforementioned object classes as shown in Fig. 2.

2.2 The methodology

When we hold an object in our palm, depending upon the shape of the object, we feel either uniform or non-uniform pressure in different regions of the palm. For an edged object, the pressure at the edges is higher than at comparatively planar regions. In brief, different objects produce different pressure distributions on the palm depending on their shape, and this is the fundamental concept of object-shape recognition from tactile images. This unique pressure distribution is reflected in the grayscale tactile images with darker regions indicating lower pressure. Different pressure regions are separated using *K-means clustering*

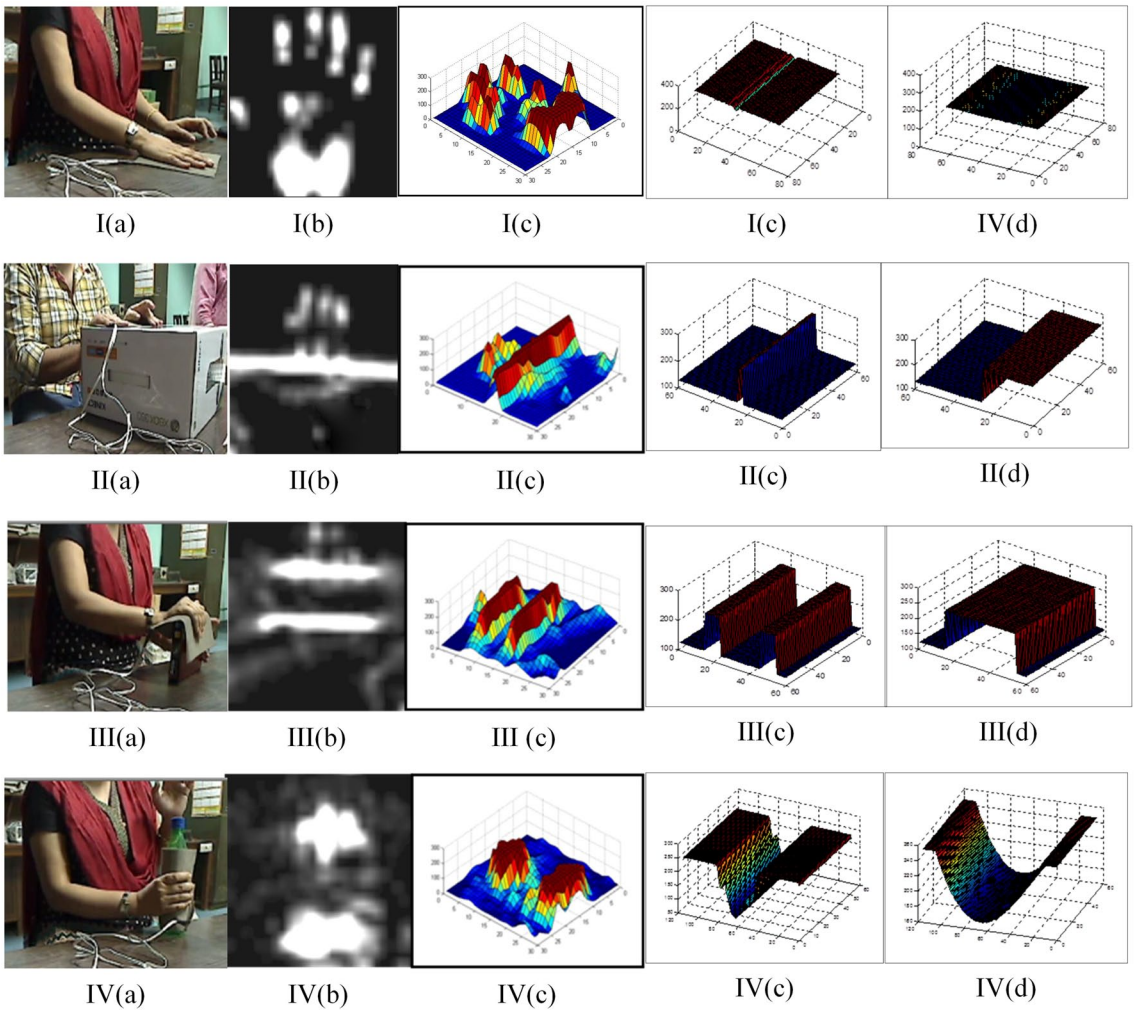

Fig. 2 **a** Object gripped, **b** image acquired and **c** raw pressure distribution for **I** Planar surface, **II** one-edged surface, **III** two-edged surface and **IV** cylindrical surface. Reconstructed surface images, the thresholding scheme for one-edged (**II**) and two-edged object (**III**) (edged objects): **d** after applying the thresholding algorithm, **e** after the postprocessing. For edgeless surfaces: the polynomial fitting scheme for planar (**I**) and cylindrical (**IV**) (edgeless objects): **d** after row-wise healing to fill the finger gaps, **e** after the polynomial fitting

[7, 13]. Then, the high-pressure regions are separated, and some regional descriptors are used to extract features for classification.

2.2.1 *Clustering different pressure regions*

Every pixel in the grayscale tactile image has an intensity value proportional to the pressure developed at that point in the palm. For an $M \times N$ image, there are a total of MN points each having intensity value in the range [0, 255]. All the points are clustered in a one-dimensional space (since every pixel has only one feature, i.e., the intensity value) using K-means clustering with $K = 3$ (number of clusters), as shown in Fig. 3. Three clusters are considered because of the existence of three distinct regions (high- and low-pressure regions and the background where pressure is nil) in the image.

2.2.2 *Feature extraction*

The rest of the analysis is carried out on the extracted high-pressure regions (HPRs) of the image as they uniquely characterize the edges and/or bends in the object. The cluster containing HPRs is separated from the other two clusters by choosing the cluster with lowest centroid value (indicating darker region in the intensity image). This is shown in Fig. 3c. The small noisy regions in Fig. 3c are eliminated by setting a minimum threshold value (50 pixels) in the area of a connected region, as shown in Fig. 3d. Then, some regional descriptors are used to extract features from these HPRs.

2.2.2.1 Regional descriptors Regional descriptor [8] features are extracted directly from the segmented (or clus-

Fig. 3 Preprocessing and clustering of different pressure regions, **a** grayscale original tactile image, **b** after clustering three clusters are formed: the *gray* regions refer to Cluster 1, i.e., low-pressure regions; the *white* regions refer to the high-pressure regions (HPRs), i.e., Cluster 2, and the *black* regions are Cluster 3 denoting background, **c** extracted high-pressure regions (HPRs) i.e., Cluster 2, containing noisy regions, **d** HPRs (i.e., Cluster 2) after elimination of noisy regions

Table 1 List of features

Feature number	1	2	3	4	5	6	7	8	9	10	11
Feature	Area (Ar)	Centroid (C)		Bounding box (BB)				Convex Hull (CH)	Eccentricity (ECC)	Euler's number (EN)	Orientation (Or)
		x_C	y_C	x_{BB}	y_{BB}	L_{BB}	W_{BB}				

tered) HPRs. It describes a unique characteristic of the segmented image. The extracted regional descriptors used are defined below:

Area (Ar): The area of a region is defined as the number of pixels in that region.
Centroid (C): It specifies the center of mass of a region. It must not be confused with the cluster centroid. It is the spatial or geometrical centroid of a region (has no relation with the intensity of that region).
Bounding box (BB): It is the smallest rectangle containing the region.
Convex hull (CH): It is the smallest convex polygon that can contain the region.
Eccentricity (Ecc): It is a scalar number that specifies the eccentricity of the ellipse that has the same second moments as the region. The eccentricity is the ratio of the distance between the foci of the ellipse to its major axis length.
Euler number (EN): The Euler number of an image is the number of connected components in that image minus the number of holes in that image. It is a topological descriptor, and it is invariant to stretching or rotation distortion (sometimes known as *rubber sheet distortions* [8]).
Orientation (Or): It is a scalar that denotes the angle (in degrees ranging from $-90°$ to $90°$) between the x-axis and the major axis of the ellipse that has the same second moments as the region.

2.2.2.2 The feature vector An eleven-length feature vector is obtained using the above regional descriptors, as shown in Table 1.

1. Total area of the HPRs (Ar).
2. X-coordinate of the centroid (x_C).
3. Y-coordinate of the centroid (y_C).
4. X-coordinate of the top-most and left-most vertex of the bounding box of all HPRs (x_{BB}).
5. Y-coordinate of the top-most and left-most vertex of the bounding box of all HPRs (y_{BB}).
6. Length of the bounding box of all HPRs (L_{BB}).
7. Width of the bounding box of all HPRs (W_{BB}).
8. Area of the convex hull containing all HPRs (CH).
9. Eccentricity of the HPRs (Ecc).
10. Euler number of the HPRs (EN).
11. Orientation of the HPRs (Or).

2.2.3 Classification

The classification is performed by linear support vector machine (LSVM) classifier. The above feature vector is computed for every tactile image. Since we have a total of 4,000 images for four object classes, 4,000 feature vectors have been extracted from them. The K-fold cross-validation is performed on the feature set with K = 5. In K-fold cross-validation, the N (=4,000) observations are randomly subdivided into K disjoint sets. First ($K-1$) (=4) sets are

used for training of the classifier (LSVM), and the last set is used for evaluation (testing).

3 3D reconstruction of object-shape

Generally, we humans tend to recognize an object in two stages. The first stage simply employs mechanical recognition of the object, which is an idea of the topology of that part of the object's surface that is in contact with the palm, i.e., enclosure [10]. This idea of the topological surface maps a visual imagery in our mind based upon the individual's previous experience of holding an object of similar shape. This is the reason why infants who have not had a prior experience of holding an object are incapable of accurately recognizing it. Since the proposed scheme mimics this attribute of human behavior, the second stage of object recognition demands reproducing an estimate of the object's 3D shape based on the topological description of the object's surface obtained in the previous stage. It is this 3D shape that will play the role of the visual imagery for recognition based on experience.

3.1 Determination of surface topology (edged or edgeless)

For edged objects, there is a sudden change of intensity at the high-pressure regions (HPRs) due to the presence of an edge. But, for an edgeless object, generally there is a gradual change in the intensity at the HPRs. This change of intensity can be measured using image gradient [8]. Hence some intensity and gradient-related features have been extracted to classify a tactile image into one of the two classes viz. (1) edged object and (2) edgeless object. The features considered are described below.

1–11	Previously described eleven regional descriptors.
12	Maximum intensity in the image.
13	Minimum intensity in the image.
14	Average intensity in the image.
15–17	Area of the high-pressure region having maximum area.
18–20	Average gradient-magnitude (G_m) [8] value of the above region. The average value for a region has been calculated by averaging over the gradient-magnitude values of all the contour pixels of that region.
21–23	Average gradient angle [8] value of the above region.

For distinguishing edged and edgeless surfaces, a gradient threshold, G_{th}, is set, which is experimentally found out to be 25. If, for a particular image, $G_m > G_{th}$, then it is an edged surface otherwise an edgeless surface.

3.2 Reconstruction of edged surfaces using *RecEdged ()*

If the object considered is determined to be edged, then the *RecEdged ()* subroutine is called to reconstruct the 3D shape of the object [Fig. 2d, e for one-edged (II) and two-edged (III)]. The image is clustered into three classes (background, high-pressure region and low-pressure region) using K-means clustering as explained before. Then, each cluster is given a particular intensity value (the mean of all the pixels in that cluster (Fig. 3b). Now, the thresholding algorithm is applied, as presented in Fig. 4a.

Here, let the grayscale image be A (of size $M \times N$), where *a(i,j)* refers to the element in *i*th row and *j*th column. Let, C_0 denotes the background cluster having intensity value I_0; C_1 be the cluster with medium intensity I_1; and C_2 be the cluster with highest intensity I_2. N_0, N_1 and N_2 denote the number of pixels in cluster C_0, C_1 and C_2, respectively. T_1 and T_2 are the row thresholding values, and K is a constant. Those images which are recognized as the tactile images for edged objects are scanned from top to bottom. The number of pixels in each cluster is calculated. If the number of pixels for a certain row *is* greater than $0.5 \times N$, (where N is total number of pixels in all the clusters), then that row is ignored, as is denotes the row mainly comprising the background pixels. If N_1 is greater than N_2, then the surface is elevated to a height of T_1 ($=K \times I_2$), as it implies the presence of an edge. The surface continues at level T_1 until the next edge is encountered, (i.e., when $N_2 > N_1$) or the end of the image is reached. Then, the surface is shifted down by a height of T_2 ($=K \times I_2$). The resulting reconstructed surface images of edged object shapes are shown in Fig. 2II(d), III(d), II(e) and III(e).

3.3 Reconstruction of edgeless surfaces using *RecEdgeless ()*

The *RecEdgeless()* subroutine is called whenever the object is edgeless. At first, the rows having mainly background pixels are eliminated as before. In a similar way, the columns having mainly background pixels are also eliminated. Then, the image is column-wise fitted with a polynomial *p(x)*. The following algorithm does not show the background elimination stage for space consideration. Let, after background elimination, the image is A_1 of size $M_1 \times N_1$, with $a_1(i_1, j_1)$ denoting the element a_1 in i_1th row and j_1th column.

The scheme is illustratively shown in Fig. 4b. Figure 2I(d), I(e), IV(d) and IV(e) are the reconstructed shapes for planar and cylindrical object, respectively.

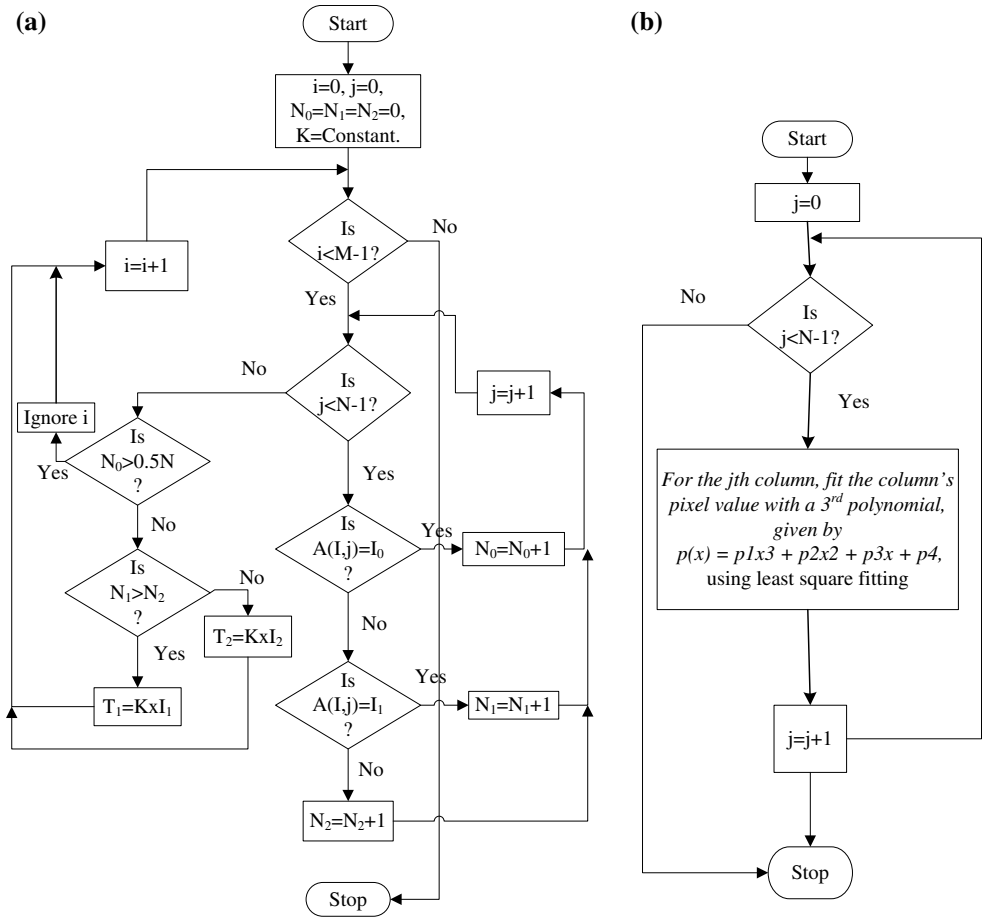

Fig. 4 The reconstruction algorithm subroutines for **a** objects with edge using *RecEdge()* subroutine and **b** edgeless objects using *RecEdgeless()* subroutine

4 The hybrid shape recognition algorithm

As discussed earlier, here our aim is to add some shape-related information to the previous 11-length regional descriptor features extracted from the preprocessed tactile image (as presented in Sect. 2.2.2) vector. Since the slope information of a surface is contained in its gradient, a gradient analysis is the prerequisite to an object's accurate shape description. Hence, the gradient-magnitude matrix for every reconstructed shape is evaluated and concatenated with the previous feature vector just as features from the visual imagery produced in the mind aid an individual to recognize an object based on previous learning experience. The previously obtained regional descriptor feature vector was a row matrix of dimension 1×11. It conceptually denotes the past learning experience. For a tactile image of size $M \times N$, the gradient matrix (which is also of size $M \times N$) is transformed into a row matrix of size $1 \times MN$. This matrix denotes the present feeling about the surface topology from the gradient information. Now, the gradient matrix ($1 \times MN$) is concatenated to the previous regional descriptor feature matrix (1×11), and a new feature vector is obtained of dimension $1 \times (MN + 11)$. This feature vector is now used for the classification purpose.

5 Results and discussion

5.1 Classification accuracy in noise-free environment

The classification results for conventional image feature-based recognition algorithm, i.e., regional feature-based classification and the hybrid recognition algorithm using LSVM classifier are shown in Table 2. From the table, it is clear that the average classification accuracy for conventional recognition is 92.6 %, while for hybrid recognition, it is 97.62 %. The run times for regional feature-based and hybrid recognition techniques are 0.476 and 0.502 s, respectively, which are comparable and can be used in real-time classification purposes. Based on the classification accuracies, it is noted that the hybrid recognition algorithm

Table 2 Classification results for normal and hybrid recognition

Object-shape classification		Object shapes			
		Planar	One-edged	Two-edged	Cylindrical
Conventional recognition	Classification accuracy (%)	100	93.46	89.73	87.21
	Mean classification accuracy (%)	92.6			
	Run time (s)	0.476			
Hybrid recognition	Classification accuracy (%)	100	98.09	96.17	96.24
	Mean classification accuracy (%)	97.62			
	Run time (s)	0.502			

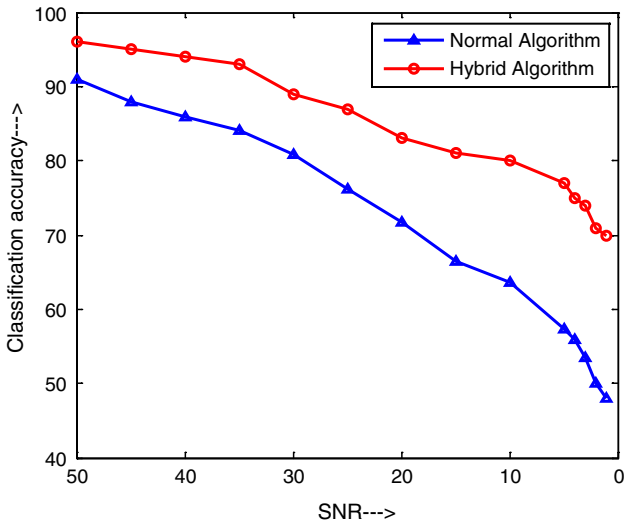

Fig. 5 Variation in classification accuracy with SNR

performs better than the regional feature-based recognition algorithm in noise-free environment.

5.2 Noise immunity

To check the noise immunity of the proposed algorithm, we have added white Gaussian noise to the feature set and then applied it to the classifier. Figure 5 shows the variation in classification accuracy with decreasing signal-to-noise ratio (SNR) for regional feature-based and hybrid shape recognition schemes. The slope of the curve obtained in the hybrid algorithm is less than that obtained in the other, which ensures lesser degradation in classification accuracy when noise corrupts the data.

5.3 Statistical test

The robustness of the proposed algorithm is tested by 5×2 cv paired t test [6]. The competitor classifiers are linear discriminant analysis (LDA) [1], support vector machine with Gaussian radial basis function (SVM-RBF kernel with a scaling factor, sigma, of 1.) [29], k-nearest neighbor (kNN) [16, 17] and feed forward neural network (FFNN) [9]. The 5×2 cv paired t test is a statistical test used to compare two supervised classification algorithms. Here, the null hypothesis assumes that the two competitor algorithms have same error rates. In this test, five replications of twofold cross-validation are performed. In each replication, the total data set is randomly divided into two sets S_1 and S_2. Now, to compare two classification algorithms A and B, each of them is trained on each set and tested on the other set.

Hence, each replication produces four error estimates: $p_A^{(1)}$ and $p_B^{(1)}$ (trained on S_1 and tested on S_2) and $p_A^{(2)}$ and $p_B^{(2)}$ (trained on S_2 and tested on S_1). Here,

$$p_A = (n_{00} + n_{01})/n \quad \text{and} \quad p_B = (n_{00} + n_{10})/n$$

where n = total number of training samples $= n_{00} + n_{01} + n_{10} + n_{11}$, $\boldsymbol{n_{00}}$ = number of samples misclassified by both A and B, $\boldsymbol{n_{01}}$ = number of samples misclassified by A but not by B, $\boldsymbol{n_{10}}$ = number of samples misclassified by B but not by A, $\boldsymbol{n_{11}}$ = number of samples misclassified by neither A but nor B. If we subtract the corresponding error estimates, then we get two estimated differences $p^{(1)}$ and $p^{(2)}$, where

$$p^{(1)} = p_A^{(1)} - p_B^{(1)} \quad \text{and} \quad p^{(2)} = p_A^{(2)} - p_B^{(2)}.$$

So, the estimated variance can be calculated as

$$s^2 = (p^{(1)} - \bar{p})^2 + (p^{(2)} - \bar{p})^2$$

Table 3 Statistical comparison: the 5×2 cv paired t test

Reference algorithm = LSVM		
Classifier algorithm used for comparison	$\lvert\tilde{t}\rvert$	Comments on acceptance/ rejection of the null hypothesis
FFNN	0.707	Accepted
kNN	1.414	Accepted
SVM-RBF	1.238	Accepted
LDA	2.122	Rejected

where $\bar{p} = \left(p^{(1)} + p^{(2)}\right)/2$. Let s_i^2 is the estimated variance for the ith replication, and $p_1^{(1)}$ is the value of $p^{(1)}$ for the first replication (out of total five replications). Then, the 5×2 cv paired $\tilde{t}$ statistic is defined as

$$\tilde{t} = \frac{p_1^{(1)}}{\sqrt{\frac{1}{5}\sum_{i=1}^{5} s_i^2}}.$$

In [6], the author proved that "under the null hypothesis, $\tilde{t}$ has approximately a t-distribution with 5° of freedom." Now, the threshold for a t-distribution with 5° of freedom is given by $t_{\text{threshold}} = \pm 2.01505$. Hence, the null hypothesis is rejected if $|\tilde{t}| > |t_{\text{threshold}}|$. Table 3 shows the acceptance or rejection of the null hypothesis after performing 5×2 cv paired t test.

From this statistical test, it can be concluded that except LDA, all the other classifiers have similar classification accuracy as LSVM since the null hypothesis is accepted for them. This proves the robustness and classifier independent nature of the proposed technique of object-shape recognition.

6 Conclusion and future direction

The article presented a scheme for object-shape recognition and 3D reconstruction from tactile images. The scheme can be suitably used for developing an artificial rehabilitation system by which an amputee would be capable of perceiving an object's shape. A regional descriptor-based shape recognition scheme has been presented along with a technique for 3D reconstruction of the portion of the object in grip. The article also proposed a hybrid recognition algorithm that is inspired by the inherent strategy of every human to recognize an object's shape. In the hybrid approach of object-shape recognition, both raw image features and reconstructed shape-related information are used for the classification purpose. It achieves an average classification accuracy of 97.62 %, while the conventional recognition scheme achieves an accuracy of only up to 92.6 %. Moreover, the proposed hybrid scheme has better noise immunity and higher robustness as is evident from its performance in the 5×2 cv paired t test.

However, the presented work has some drawbacks. Firstly, the object gripping has been performed by human palm because of the lack of proper robotic palm. But, this would not create so much problem since the efficacy of the algorithm will be preserved when artificial robotic palm [22–26] having human-palm like characteristics will be used. Secondly, at the initial stage of the research, only four object classes have been considered. Obviously, the recognition accuracy will deteriorate when number of objects will be increased. But, the results obtained by experimenting on this small set of objects prove the fact that the hybrid recognition strategy, mimicking the human technique of recognition, is capable of recognizing the objects with far better accuracy than the conventional recognition techniques and also fast for real-time applications. Thirdly, the reconstruction algorithm (which has been effectively used for reconstructing simple geometrical shapes only from the raw pressure distribution pattern) cannot be directly applied on complex-shaped object for reconstruction purpose. However, a complex-shaped object can be seen as a combination of a number of simple shapes. Thus, in future, we can capture multiple tactile images at different portions of the object along with data from position or displacement sensors to be placed on the fingers, to reconstruct the complete 3D structure of the objects.

Keeping intact the novelty of our approach, our next step would be hardware realization of the scheme using pressure sensors fit on an artificial robot hand and developing vibrotactile feedback system in order to accomplish our objective of creating a usable real-time system capable of perceiving the accurate shape of an object for rehabilitative purposes and human–computer interaction (HCI) applications.

Acknowledgments This study has been supported by University Grants Commission (UGC), India, University with Potential for Excellence—Phase II (UPE II) in Cognitive Science, Jadavpur University and Council of Scientific and Industrial Research (CSIR), India.

References

1. Alpaydin E (2004) Linear discrimination. Introduction to machine learning, 1st edn. MIT Press, Cambridge, pp 197–228
2. Argall BD, Billard AG (2010) A survey of tactile human-robot interactions. Rob Auton Syst 58(10):1159–1176
3. Bierbaum A, Gubarev I, Dillmann R (2008) Robust shape recovery for sparse contact location and normal data from haptic exploration. In: IEEE/RSJ international conference on intelligent robots and systems (IROS 2008). IEEE, Nice, pp 3200–3205
4. Chia-Ping C, Chu-Song C, Yi-Ping H (2009) Pixel-based correspondence, and shape reconstruction for moving objects. In: Proceedings IEEE 12th international conference on computer vision workshops (ICCV workshops). IEEE, Kyoto, pp 1962–1969
5. Dahiya RS, Metta G, Valle M, Sandini G (2010) Tactile sensing: from humans to humanoids. IEEE Trans Rob 26:1–20
6. Dietterich TG (1998) Approximate statistical test for comparing supervised classification learning algorithms. J Neural Comput 10(7):1895–1924
7. Duda RO, Hart PE, Stork DG (2012) Unsupervised learning and clustering. In: Pattern classification. Wiley, New York, pp 517–600
8. Gonzalez RC, Woods RE, Eddins SL (2012) Digital image processing using MATLAB, 4th edn. Tata McGraw Hill, LLC, USA, pp 551–614

9. Graupe D (2007) Principles of artificial neural networks, 2nd edn. Advanced series on circuits and systems, vol 6. World Scientific, Denver, MA
10. Ballesteros S, Heller MA (2008) Haptic object identification. In: Grunwald M (ed) Human haptic perception. Basics and Applications. Birkhauser Basel, Birkhauser Verlag AG, pp 207–222
11. Hayward V, Astley OR, Cruz-Hernandez M, Grant D, Robles-De-La-Torre G (2004) Haptic interfaces and devices. J Sens Rev 24:16–29
12. Heidemann G, Schopfer M (2004) Dynamic tactile sensing for object identification. In: Proceedings of IEEE international conference on robotics and automation (ICRA '04), vol 1. IEEE, New Orleans, LA, pp 813–818
13. Jain AK, Murty MN, Flynn PJ (1999) Data clustering: a review. ACM Comput Surv, N. Y., U. S. A. 31(3):264–323
14. Khasnobish A, Jati A, Singh G, Bhattacharyya S, Konar A, Tibarewala DN, Kim E, Nagar AK (2012) Object-shape recognition from tactile images using a feed-forward neural network. In: Proceedings IEEE international joint conference on neural networks (IJCNN 2012). IEEE, Brisbane, QLD, pp 1–8
15. Meier M, Schopfer M, Haschke R, Ritter H (2011) A probabilistic approach to tactile shape reconstruction. IEEE Trans Rob 27:630–635
16. Mitchell T (1997) Instance based learning. In: Machine learning. McGraw Hill, New York, pp 239–258
17. Murphy OJ (1990) Nearest neighbor pattern classification perceptrons. In: Proceedings of the IEEE, vol 78. IEEE, pp 1595–1598
18. Nakamoto H, Fukui W, Kobayashi F, Kojima F, Imamura N, Shirasawa H (2009) Shape classification based on tactile information by universal robot hand. In: 35th annual conference of IEEE on industrial electronics (IECON '09). IEEE, Porto, pp 2360–2365
19. Okamura AM, Turner ML, Cutkosky MR (1997) Haptic exploration of objects with rolling and sliding. In: Proceedings of the IEEE international conference on robotics and automation, vol 3. IEEE, Albuquerque, NM, pp 2485–2490
20. Pezzementi Z, Plaku E, Reyda C, Hager GD (2011) Tactile-object recognition from appearance information. IEEE Trans Rob 27:473–487
21. Romano JM, Hsiao K, Niemeyer G, Chitta S, Kuchenbecker KJ (2011) Human-inspired robotic grasp control with tactile sensing. IEEE Trans Rob 27:1067–1079
22. Shimoga KB, Goldenberg AA (1996) Soft robotic fingertips part II: modeling and impedance regulation. Int J Rob Res 15(4):335–350
23. Sigiuchi H, Watanabe S, Hasegawa Y, Nornoto M (2000) A control system for multi-fingered robotic hand with distributed touch sensor. In: 26th annual conference industrial electronics society, IECON 2000, vol 1. IEEE, Nagoya, pp 434–439
24. Simpkins A (2013) Robotic tactile sensing: technologies and system (Dahiya RS, Valle M 2013) [on the shelf]. IEEE Robot Autom Mag 20(2):107–107
25. Takamuku S, Fukuda A, Hosoda K (2008) Repetitive grasping with anthromorphic skin-covered hand enables robust haptic recognition. In: International conference on intelligent robots and systems (IROS 2008). IEEE, Nice, pp 3212–3217
26. Talasaz A, Patel RV (2013) Integration of force reflection with tactile sensing for minimally invasive robotics-assisted tumor localization. IEEE Trans Haptics 6:217–228
27. Ting Z, Hong L, Li J, Shaowei F, Jing Y (2013) Development of a flexible 3-D tactile sensor system for anthropomorphic artificial hand. IEEE Sens J 13:510–518
28. Visell Y (2009) Tactile sensory substitution: models for enaction in HCI. J Interact Comput 21:38–53
29. Webb AR, Copsey KD (2011) Nonlinear discriminant analysis—kernel and projection methods. In: Statistical pattern recognition, 3rd edn. Wiley, New York, pp 274–321
30. Yamada Y, Ishiguro A, Uchikawa Y (1993) A method of 3D object reconstruction by fusing vision with touch using internal models with global and local deformations. In: Proceedings international conference on robotics and automation, vol 2. IEEE, Atlanta, GA, pp 782–787